IOP Publishing Journal of Physics: Condensed Matter
J. Phys.: Condens. Matter **32** (2020) 205901 (11pp) https://doi.org/10.1088/1361-648X/ab6e96

Searching high spin polarization ferromagnet in Heusler alloy via machine learning

Xiao Hu[1], Yaqiong Zhang[1], Shuaiyu Fan[1], Xin Li[1], Zhenjie Zhao[1], Chao He[2], Yonghong Zhao[2], Yong Liu[3] and Wenhui Xie[1]

[1] Engineering Research Center for Nanophotonics and Advanced Instrument, School of Physics and Electronic Science, East China Normal University, Shanghai 200062, People's Republic of China
[2] College of Physics and Electronic Engineering, Center for Computational Sciences, Sichuan Normal University, Chengdu 610068, People's Republic of China
[3] State Key Laboratory of Metastable Materials Science and Technology & Key Laboratory for Microstructural Material Physics of Hebei Province, School of Science, Yanshan University, Qinhuangdao 066004, People's Republic of China

E-mail: yongliu@ysu.edu.cn or mailto: ycliu@ysu.edu.cn and whxie@phy.ecnu.edu.cn

Received 10 December 2019, revised 29 December 2019
Accepted for publication 22 January 2020
Published 20 February 2020

Abstract

In order to search for stable ferromagnets with high spin polarization in Heusler alloys for spintronic applications, we develop an efficient machine learning workflow based on a deep neural network, whose training data were collected from the open quantum materials database and high throughput calculation by first-principle calculations. The lattice constants, formation energy and spin polarization of 10 577 candidate materials were predicted, and 192 materials with high spin polarization were selected according to a spin polarization greater than 0.87 and formation energy less than 80 meV/atom. 57 of these alloys have been reported as Half-metal (100% spin polarization) according to previous researches, and 18 have been reported as semiconductors. Especially, 6 Heusler alloys were identified as promising half-metallic ferromagnets, and some of them have high Curie temperature above room temperature. Our study suggests this approach is an efficient method for the discovery of superior spintronic materials, which should be also suitable for exploring other functional materials.

Keywords: Heusler alloys, spintronic, half-metallic ferromagnet, machine learning

Supplementary material for this article is available online

(Some figures may appear in colour only in the online journal)

1. Introduction

Considerable interest is now devoted to the search for novel ferromagnetic (FM) materials suitable for application in spintronics [1, 2]. For effective spin injection of semiconductors, these materials usually possess a very high spin polarization (HSP) of the electron states [3, 4], especially half-metal with 100% spin polarization at the Fermi level ($P_F = 1$), such as some Heusler alloys [5], zinc-blende structure compounds [6], CrO_2 [7] and Fe_3O_4 [8]. Meanwhile, these materials must have a Curie temperature (T_C) noticeably higher than the room temperature to be compatible with the semiconductors used in industry [9]. Of them all, Heusler alloys are attractive materials with various fantastic properties such as superconductor, topological insulators, Kondo systems and heavy-Fermion behavior [10–13]. In particular, many half-metals (HM) with high T_C, which even more than several hundred degrees above room temperature [14, 15], have been found in Heusler alloys, thus always attracted extensive attention.

Exhausting investigations have been carried out in the past several decades, then many excellent ferromagnetic Heulser alloys had been excavated. Recently, Sanvito *et al*

systematically studied the thermodynamical stability and magnetic properties of Heusler alloys made of transition metals with the assist of high throughput calculations to search high T_C compounds [16]. Obviously, expensive computing resources should be needed in order to screen all candidate materials due to the exponentially increasing complexity with a variety of chemical compositions. In fact, there are already many efforts underway, which have led to a boom in very useful materials science databases such as materials project [17], AFLOWlib [18], and OQMD [19]. In spirit of statistical learning or machine learning (ML), the leading paradigm is that, incorporating with first-principles computational methods, such as density functional theory (DFT), researchers populate and analyze the computational materials databases and the massive data from published literature to screen candidate materials for target properties, which significantly reduced the computing cost [20–22].

So far, machine learning as an effective method has been attracting much attention in the field of material science. For example, Kernel ridge regression as an efficient regression model is used to estimate molecular energy [23] and find density functional [24]; Random forest method [25, 26] and support vector machine [27] were as used to judge the material structure. At the same time, the ML methods based on deep neural network (DNN) are also prominent, from finding atomic topology in crystals [28] to analyzing complex reaction networks to guide experimental design [29], and predicting crystal stability [30, 31], although it is less interpretable than other methods. These reveal that DNN has fantastical success due to robust feature extraction and function fitting ability, thus it may help us achieve mass data analysis and search for emerging materials rapidly [17, 32, 33]. However, the discovery of stable HSP ferromagnet in this way has not been reported yet.

In this paper, we design a workflow composed of multiple DNN models to predict lattice constants, formation energy and spin polarization, as illustrated with figure 1, which are utilized to search for stable HSP materials. The reason for using three models here is because they have different characteristics, which are also necessary to implement in different training sets and validation sets. Firstly, if an alloy is expected to form in the desired structure, it is necessary to verify the lattice constants with high precision by comparing it with the database of x-ray after experimentally synthesized or the DFT calculated data. Secondly, the formation energy is essential to the synthesis and stability of materials, but it is not easy to obtain formation energy data through experimental methods, and calculation of formation energy is also complex. If we can predict the formation energy of materials, excluding materials that cannot be synthesized can greatly reduce the search scope of materials with high spin polarization. Thirdly, the spin polarization P_F is much hard to obtain experimentally, but it could be easily extracted from first-principle DFT calculation. Meanwhile, despite the exploding growth of the number of compiled entries of computational materials database currently, rarely materials have been known for the information of P_F. Therefore an independent data set via first-principle DFT calculations has to be constructed for training and testing.

We only focused on the A_2BC trinary compounds, which consist of full-Heusler and inverse Heusler structure, shown in figures 2(a) and (b). The input required for the entire workflow is also terse, which only includes the name of the three elements that make up the Heusler alloy. Finally, there were 192 stable HSP materials were figured out in 10 577 materials. Furthermore, with the assistance of first-principles calculation by DFT, 6 alloys were identified to behave half-metallic and were discussed in detail. The paper is organized as follows: in section 2, we present the details of our methods. The source of data set is described in the section 2.1. The parameters setting of the DNN training and the descriptors are described in section 2.2. The calculation details of the first principle calculation are given in the section 2.3. In section 3.1, the accuracy of three DNN models is analyzed and the process of searching HSP and HM materials using DNN models is presented. Then the results and discussions are presented in section 3.2.

2. Method

2.1. Introduction of data set

In this work, we used many data sets, and detailed information about their sources and roles can be found in table 1. The first data set comprise 10 577 candidate materials, which initially contain only the name of materials, and are needed to predict their lattice constant, formation energy and spin polarization via DNN models. A- and B-site atoms are 3d, 4d, 5d transition metals excluding radioactive elements, and used Al, Si, P, S, Mg, Ar, Ga, Ge, As, Se, B, In, Sn, Sb as the C-site atoms. These elements consist of the target area of the Periodic table that we are interested in, in which we attempt to find stable HSP ferromagnets.

Next, approximately 65 000 Heusler alloys were collected from the open quantum materials database (OQMD) [19], including the information about the structure and formation energy. There are certain criteria for the selection of the three elements that make up the Heusler alloys, which A- and B-site atoms from 3d, 4d, 5d periods and C-site atoms from groups III–VI. However, we excluded hydrogen and inert gas elements that are considered difficult to form stable compounds. Also, radioactive lanthanides and actinides elements are not included. The collection conditions of this data set appear to be similar to the data set of 10 577 materials, but the content is quite different. We get 65 000 materials data based on these conditions, but the random combination is not sure to find the corresponding material in the database. However, for the data set of 10 577 materials, we can determine a material based on the random combination. Therefore, among 65 000 materials, only 1506 materials overlapped with 10 577 candidate materials, which were removed in the training process and used for comparing with the predicted results of the model, and nearly 9000 of the 10 577 materials were not found in the data set of 65 000 materials.

Furthermore, we prepared a data set containing 3450 materials to train the model of spin polarization. We selected 17 transition metals as A- or B-site atoms, including Sc, Ti, V, Cr, Mn, Fe, Co, Ni, Cu, Zn, Y, Zr, Nb, Mo, Ru, Rh, Pd, and the

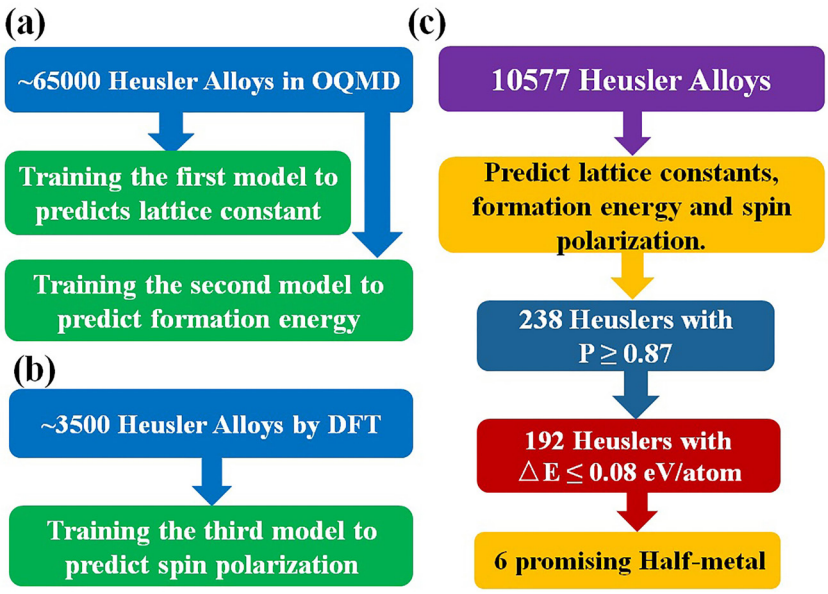

Figure 1. Our workflow for models training and searching HSP Heusler alloys. (a) The data for training the first and second models comes from OQMD. The first model is used to predict lattice constant, and the second is used to predict formation energy. (b) The data for training the third model comes from high throughput calculation. The third model is used to predict spin polarization. (c) By screening candidate materials with spin polarization greater than 0.87 and formation energy less than 80 meV/atom, we found promising six half-metallic materials finally.

selection of C- site atom is the same as the previous candidate materials data set. The data set is derived from the results of first-principle spin-polarized calculation, and details would be introduced in the following. To verify the spin polarization model, we randomly selected 119 materials as test set from 10 577 materials and obtained their P_F via the first-principle calculation.

The full-Heusler alloy crystallizes in the cubic space group Fm-3m (space group *No*.225) with Cu_2MnAl (L21) as the prototype. The A-site atoms occupy the Wyckoff position 8c (1/4, 1/4, 1/4), the B- and C-site atoms are located at 4a (0, 0, 0) and 4b (1/2, 1/2, 1/2), respectively (figure 2(a)). Inverse Heusler structure is still described by four interpenetrating fcc sublattices, and A-site atoms are placed on the Wyckoff positions 4a (0, 0, 0) and 4d (3/4, 3/4, 3/4), while the B- and C-site atoms are located at 4b (1/2, 1/2, 1/2) and 4c (1/4, 1/4, 1/4), respectively (figure 2(b)). Although the data set include both the full-Heusler and inverse Heusler alloys, unfortunately, our model could not distinguish the structure during the training process, since the discrepancy of the formation energy between two structures is often quite tiny. Thus, we only distinguish the structure after capturing a stable HSP ferromagnet.

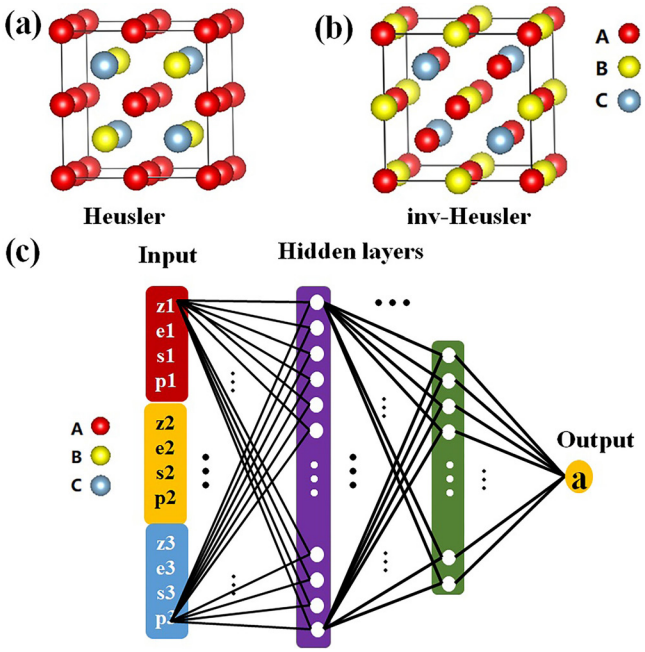

Figure 2. The structure of Heusler alloy: (a) Heusler and (b) inverse Heusler structures, that created by VESTA. (c) Schematic diagram of multilayer fully connected neural network.

2.2. Details of DNN model

As shown in table 2, we selected some descriptors as model's inputs. Descriptors are derived from the atomic information of the elements that make up the material and do not require any first-principle calculations. The selection of descriptors is based on previous researches [23, 26, 34] or semi-empirical approaches. For example, the atomic number should be important for the prediction of the lattice constant, while the electronegativity and unit cell size would significantly influence on the formation energy.

We design three models according to the different characteristics of prediction properties, and they have different descriptors: *(a)* We get the first model that can predict the value of lattice constant by using the atomic number, the number of core electron, the number of s-orbital electron and

Table 1. The data set used in this work.

	Size	Source	Purpose	Caption
a	64 935	OQMD	Model training	A- and B-site atoms from 3d, 4d, 5d periods and C-site atoms from groups III–VI
b	3450	DFT	Model training	A- or B- site atoms include Sc, Ti, V, Cr, Mn, Fe, Co, Ni, Cu, Zn, Y, Zr, Nb, Mo, Ru, Rh, Pd, and used Al, Si, P, S, Mg, Ar, Ga, Ge, As, Se, B, In, Sn, Sb as the C-site atoms
c	10 577	By ourselves	Search for HM	This database only contains the names of material. A- and B-site atoms are 3d, 4d, 5d transition metals excluding radioactive elements, and Al, Si, P, S, Mg, Ar, Ga, Ge, As, Se, B, In, Sn, Sb as C-site atoms
d	1506	OQMD	Test set	The overlap of set *a* and set *c*
e	119	DFT	Test set	Randomly selected from 10 577 materials

Table 2. Descriptors of DNN model. The descriptors using in the first model are a, b, c, d and e. When training the second model, the descriptors are a, b, c, d, e and h. The third model uses a, b, e, f and g.

	Descriptors	Symbol
a	Atomic number	z1, z2, z3
b	The number of core electron	e1, e2, e3
c	The number of s-orbital electron	s1, s2, s3
d	The number of p- or d-orbital electron	p1, p2, p3
e	Electronegativity	ele1, ele2, ele3
f	The sum of the valence electrons	ve1,ve2, ve3
g	Valence electron concentration	n
h	Lattice constant	a

the number of p- or d- orbital electron of the three elements that make up the Heusler alloy as the descriptors and lattice constants as labels. *(b)* The electronegativity of the atoms and lattice constant was added to the former descriptors, and the second model could predict the formation energy. *(c)* The atomic number, the number of core electron, the sum of the valence electrons of each atom and valence electron concentration were selected as descriptors for the third model to predict spin polarization, which is the average number of valence electrons. In the preparation of the descriptor, we did not use the first-principles calculation, focusing on the simplest information to complete the training.

Next, according to the structure of neural network, we will show how they are built and work. Three models are all neural networks composed of multiple fully connected hidden layers, as shown in figure 2(c). The input is made up of descriptors for the three elements that make up the Heusler alloy, for example, $X = (z1, e1, s1, p1, z2, ..., s3, p3)$ as the input of model for predicting lattice constants. Data were normalized by the Min-Max normalization method before the training began. The training data of each model were randomly divided into non-intersecting training sets and validation sets in proportions. The objective of model training is to minimize the loss function $L(y_{\text{pred}}, y_{\text{true}})$, where y_{true} represents the true labels and y_{pred} represents the predicted ones. We chose the L2 regular loss function, which is the sum of the squares of the between the true value and the predicted value.

$$L = \sum_{i=1}^{n} (y_{\text{pred}} - y_{\text{true}})^2. \tag{1}$$

$$f(x_{i,j}) = h(\sum_{j=1}^{n_i} w_{i-1,j} f(x_{i-1,j}) + b_{i-1,j}). \tag{2}$$

Equation (2) is the calculation formula of the neuron j in the hidden layer i. $h(y)$ is activation function, $w_{i-1,j}$ is the weight of the upper neuron, and $b_{i-1,j}$ is bias. The deep neural networks are implemented by the TensorFlow platform. The $tf.random\_normal$ function is used to initialize the network parameters (w and b) according to the normal distribution, and network parameters are optimized by Backpropagation to minimize the loss function on the training data. We use the AdamOptimizer [35] provided by TensorFlow to control the learning speed. The activation function $h(y)$ is rectified linear (ReLu) activation functions. Each network is trained until the loss function evaluated on the validation set fails to decrease after some training epochs. More detail about three models, such as the number of layers and nodes of the neural network, batch size and learning rate, are presented in table 3.

2.3. Details of DFT computation

The first-principle calculations were performed using density functional theory (DFT) method with projector augmented wave (PAW) [36] pseudopotentials implemented in Vienna *ab initio* simulation package (VASP) [37]. We select the generalized-gradient approximation Perdew–Burke–Ernzerhof (GGA-PBE) as exchange-correlation functional [38] and use a k-mesh of $12 \times 12 \times 12$. The plane wave cutoff energy is set to 400 eV. Atomic positions were fully relaxed until the energy and force were converged to 10^{-6} eV and 10^{-4} eV Å^{-1}. In addition, a much dense k-mesh of $20 \times 20 \times 20$ was used to the self-consistent calculations when dealing with six promising half-metallic materials.

Table 3. Neural network structure and training information of three models.

Details		Model A	Model E	Model P
Structure	Type	Neural Network (NN)	NN	NN
	Input (Descriptors)	z1, e1, s1, p1, eg1, z2, e2, s2, p2, eg2, z3, e3, s3, p3, eg3	z1, e1, s1, p1,eg1, z2, e2, s2, p2, eg2, z3, e3, s3, p3, eg3,a	z1, e1, ve1, eg1, z2, e2, ve2, eg2, z3, e3, ve1, eg3, n
	Number of hidden layers	5	7	5
	Number of nodes	150, 120, 90, 45, 15	200, 180, 160, 120, 90, 45, 25	50, 100, 90, 45, 15
	Output	Lattice constant	Formation energy	Spin polarization
	Activation function	ReLu	ReLu	ReLu
	Loss function	L2	L2	L2
Train	Data set size	∼63 000	∼63 000	3450
	Split train/ validation set	99%/1%	99%/1%	99%/1%
	Validation set	634	634	34
	Test set	1506	1506	119
	Learning rate	0.001	0.001	0.001
	Batch size	120	100	50

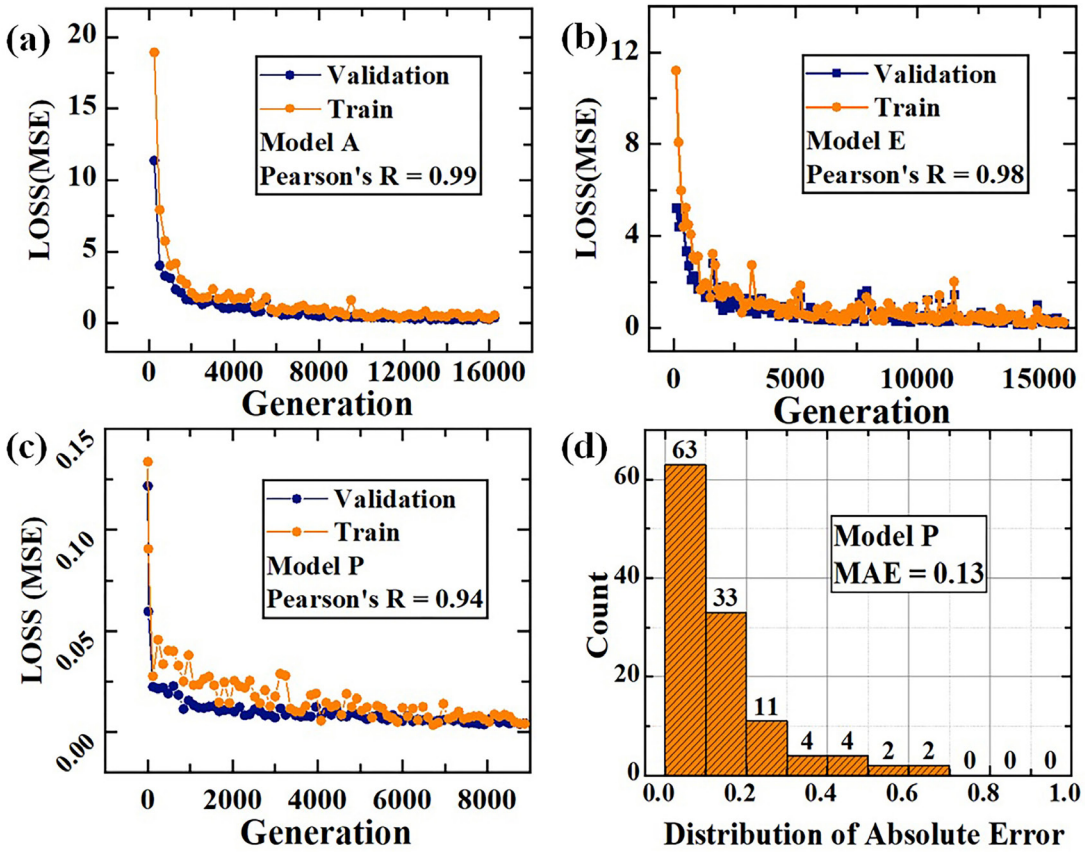

Figure 3. The value of Train- and Validation- loss function vary with generation number: (a) Model A; (b) Model E; (c) Model P. (d) The absolute error distribution of Model P.

3. Results and discussion

3.1. Performance of models

For different targets, we chose three models that performed best during training to further evaluate their predictive performance, named Model A, Model E and Model P. The value of the Pearson correlation coefficient (Pearson's R) is considered a score for the predictive performance of the three models, showing the correlation between the predicted value and the real value of a random test sample set. Pearson's R of Model A, Model E and Model P are 0.99, 0.98 and 0.94, respectively. As shown in figure 3, the value of the validation loss function is always lower than the training loss function, and decreases

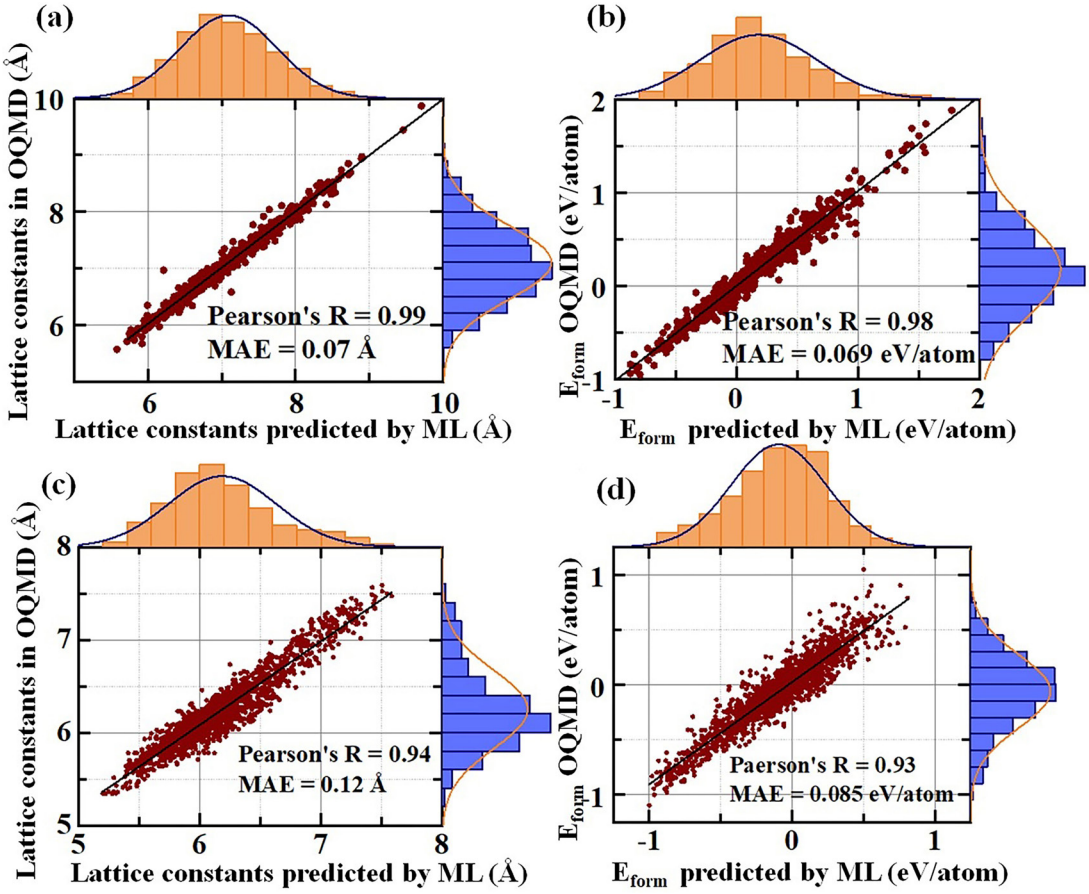

Figure 4. Comparison of lattice constants from OQMD and ML in validation set (a) and test set (c). Comparison of formation energy from OQMD and ML in validation set (b) and test set (d).

with the increase of generation number, which means that their training process are not overfitting. When the loss function reduces to a value and does not change after some generations to make sure that each sample is trained, the training process stops.

Next, we need to further evaluate the accuracy of these models. Figure 4 reveals the effectiveness of Model A and Model E in validation set and test set. The predicted results by ML were compared with the results of validation set (including 634 materials) and test set (including 1506 materials), and more information about data set can be found in tables 1 and 3. As can be observed in figures 4(a) and (b), Model A and Model E performed well in validation set, and this is the result of the last generation of the training process. The MAE of Model A is 0.07 Å, MAE of Model E is 0.069 eV/atom. The robustness and accuracy of model training may not be fully demonstrated only by analyzing validation set, so we also used a larger test set including 1506 materials. These data are overlaps between candidate materials and 65 000 materials in OQMD, which are eliminated during training and used for testing the performance of model. As shown in figures 4(c) and (d), the MAE of Model A rose slightly to 0.12 Å, that of Model E also rose to 0.085 eV/atom. In previous studies [28], the average absolute error range of prediction formation energy was in the range of 0.04–0.08 eV/atom. Our Model E is not prominent, but given the brevity of the descriptors used, the result seems acceptable. It is worth mentioning that Kirklin *et al* [19] reports that the MAE of the DFT calculation with respect to experimental measurements in OQMD is 0.081–0.136 eV/atom depending on whether the energies of the elemental reference states are fitted.

How to determine the stability of the material is the main problem to be solved in the screening of a large number of candidate materials. A common criterion [39] for stability is the difference between the total energy of the compound and that of its elementary constituents is less than 0:

$$E_{A_2BC} = \frac{E_{\mathrm{TOT}} - 2E_A - E_B - E_C}{4}. \tag{3}$$

In fact, A_2BC can be broken down into stabler binary or ternary compounds, so the most rigorous way is to construct a ternary convex hull diagram. It takes about 10 000 prototypes to construct a phase diagram of a binary alloy information diagram, and at least 30 000 to construct a ternary alloy [16, 40]. Considering that we need to screen a large number of materials, it is impossible to carry out such a huge amount of calculations. In addition, the record of convex hull energy in various databases is limited, so we still choose formation energy as a criterion for thermal stability. Perhaps after narrowing down the scope of the search, we can use the existing database for further analyzing convex hull energy.

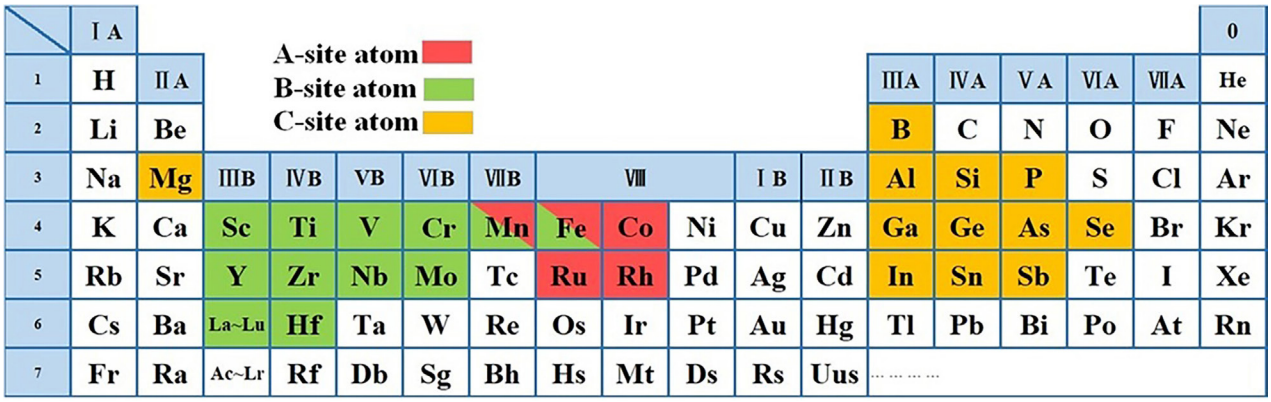

	IA												IIIA	IVA	VA	VIA	VIIA	0
1	H	IIA									IB	IIB						He
2	Li	Be											B	C	N	O	F	Ne
3	Na	Mg	IIIB	IVB	VB	VIB	VIIB	VIII			IB	IIB	Al	Si	P	S	Cl	Ar
4	K	Ca	Sc	Ti	V	Cr	Mn	Fe	Co	Ni	Cu	Zn	Ga	Ge	As	Se	Br	Kr
5	Rb	Sr	Y	Zr	Nb	Mo	Tc	Ru	Rh	Pd	Ag	Cd	In	Sn	Sb	Te	I	Xe
6	Cs	Ba	La~Lu	Hf	Ta	W	Re	Os	Ir	Pt	Au	Hg	Tl	Pb	Bi	Po	At	Rn
7	Fr	Ra	Ac~Lr	Rf	Db	Sg	Bh	Hs	Mt	Ds	Rs	Uus	...	...	...	...		

Figure 5. The distribution of components of high spin polarization materials in the Periodic Table of Elements, predicted by the DNN model. The A-site atoms are more likely to be Cr, Mn, Fe, Co, Ru, Rh, while the B-site atoms are mostly elements in the early transition metal.

Now, we begin to analyze the performance of Model P. Spin polarization [41–43] reflects the ability of a metal to maintain spin-polarized currents. The spin polarization of 3450 materials was calculated based on DFT using the following equation:

$$P_{\mathrm{F}} = \frac{n_{\mathrm{F}}^{\uparrow} - n_{\mathrm{F}}^{\downarrow}}{n_{\mathrm{F}}^{\uparrow} + n_{\mathrm{F}}^{\downarrow}} \tag{4}$$

wherein $n^{\sigma_{\mathrm{F}}}(\sigma = \uparrow, \downarrow)$ is the density of state at the Fermi level, and the up and down arrows indicate different spin directions. We got the third model by training the spin polarization of 3450 materials until the loss function value drops below 0.005, and remains stable within 500 generations without over-fitting as shown in figure 3(c). At the same time, the correlation coefficient of test results was 0.94. We also used a data set containing 119 materials to verify the model and got the absolute error distribution diagram (figure 3(d)). The MAE of the model is 0.13, which is one of the reasons why we set the screening value of HSP materials as 0.87. Because of HM has 100% spin polarization ($P_{\mathrm{F}} = 1$), the search cut-off of high spin-polarization materials was set to 0.87 to ensure that as much HM materials were found as possible. The process of searching HSP or HM materials is accelerated by checking the value of P_{F}.

3.2. Discovery of high spin polarization ferromagnets

Different from those high-throughput screening methods in which the whole chemical space should be searched at DFT level, we developed ML and DFT combined scheme only needs to compute the most promising candidate at DFT level, which greatly saves the computational resources. With these trained models, the stable HSP materials could be discovered in any target data set, including 10577 candidates in our case. As shown in figure 1(c), the lattice constants of all materials were predicted firstly, further the predicted results were added to the second model as new descriptors to forecast the formation energy, which benefits from the small MAE of model A. The spin polarization of candidate materials are given by Model P. Finally, we found 238 of all candidate materials with $P_{\mathrm{F}} > 0.87$, and 192 stable materials with the formation energy less than or equal to 80 meV. Here, we use the tolerance of $E \leqslant 80$ meV/atom to evaluate stability for two reasons: first, the MAE of Model E is close to 0.08 eV/atom; second, this criterion is used in previous study [44], which is further supported by the materials known to be stable in experiments. All predicted stable Heulser alloys are listed in supplementary information (stacks.iop.org/JPhysCM/32/205901/mmedia). By analyzing the composition of these materials as shown in figure 5, obviously, the A-site atoms are more likely to be Cr, Mn, Fe, Co, Ru, Rh, while the B-site atoms are mostly elements in the early transition metal.

It should be mentioned that 57 of these HSP stable materials have been investigated in the literature as HM or nearly HM, and 18 materials are semiconductors. The model identifies the semiconductor as HM mainly because $n_{\mathrm{F}}^{\uparrow}$ and $n_{\mathrm{F}}^{\downarrow}$ of the semiconductor are both 0. According to the formula, the spin polarization is denoted as 1. Semiconductors and HMs can be further classified in other ways. Subsequently, we performed more systematic DFT calculations to investigate their properties with different magnetic states. In the end, we found 6 promising HMs with a calculated half-metallic gap above 0.1 eV, which are Co_2NbAl, Fe_2CrGe, Co_2ScSi, Co_2CrB, Co_2ZrAl and Co_2ZrGa.

It is confirmed that Co_2NbAl, Co_2CrB, Co_2ZrGa, Co_2ZrAl, and Co_2ScSi behave FM ground state. As for Fe_2CrGe (figure 6(c)), although the electronic structure of FM state shows half-metallic behavior with a half-metal gap size of 0.346 eV, it is found that the total energy of AFM Fe_2CrGe is energy favorable. However, it is found that the ground state of Fe_2CrGe could transform to the FM state under $\pm 1.61\%$ stress on a-axis, which means that Fe_2CrGe may achieve half-metallic ferromagnetism on the thin film due to the stress induced by the substrate. It is needed to point out that the total energy difference between the FM and AFM ground states of Fe_2CrGe is only 6.4 meV/atom, which is lower than the MEA of energy ML model. Therefore, we do not consider using ML model to determine whether FM or AFM state is more stable, which would be distinguished after the screening process. The method of distinguishing different magnetic states is expected to be solved in future work.

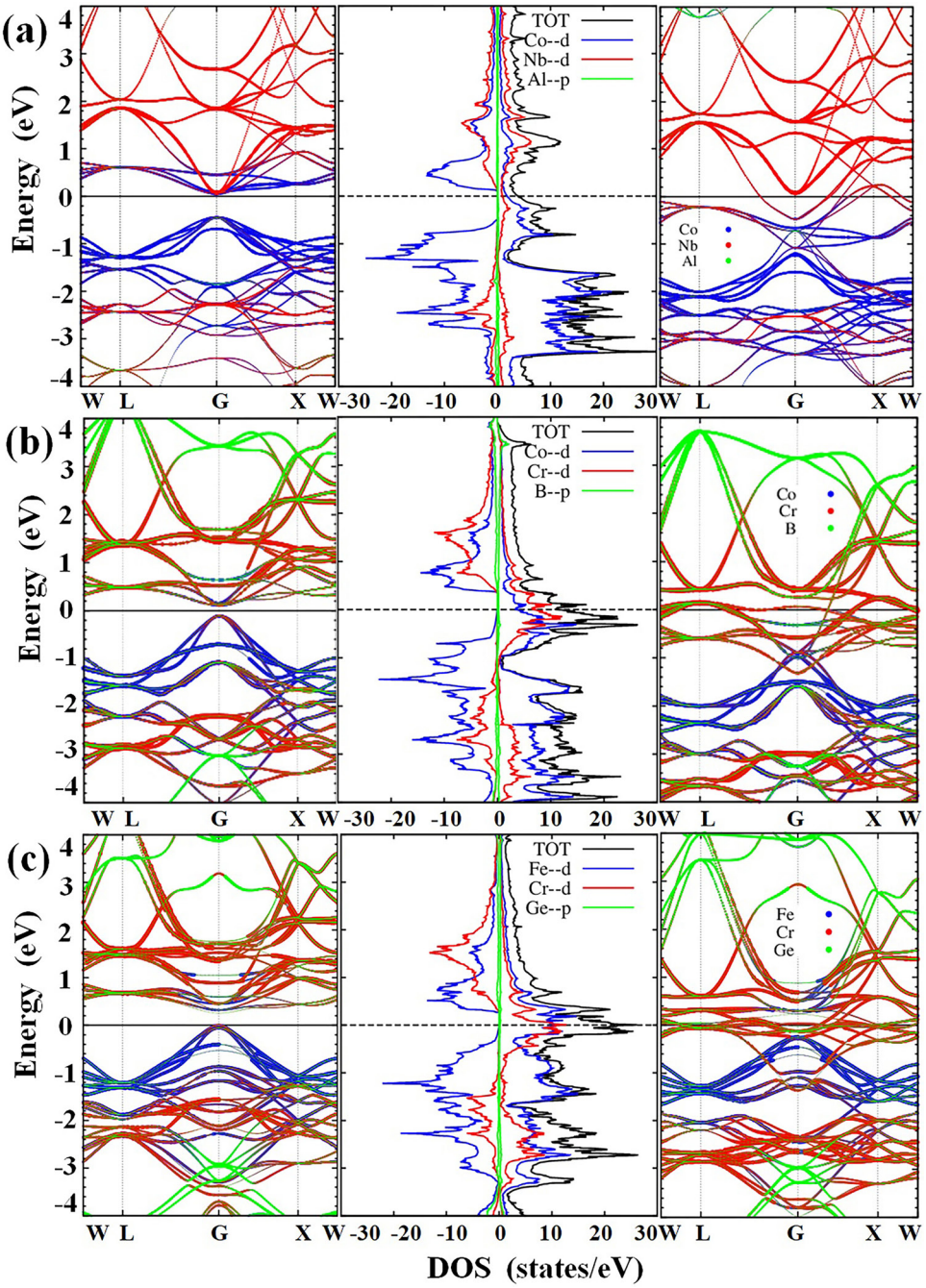

Figure 6. Band structure and DOS of Co_2NbAl, Co_2CrB and Fe_2CrGe by first-principle electronic structure calculations. The left panel shows the band structure of the minority spin channel and the right one displays the majority spin channel. The left side of middle panel shows the PDOS of the minority spin channel and the right one is majority spin channel. The zero energy is assigned to the Fermi level.

Table 4. The ground state, half-metallic gap and Curie temperature (T_C) of the six half-metal Heusler alloys are provided by DFT calculations. The formation energy (E_{Form}) are obtained from OQMD, and $E_{Form-ML}$ is predicted by Model E. Note: the estimated T_C of Fe_2CrGe responds to a distorted structure with FM states with $\pm 1.61\%$ stress on a-axis.

Name	Ground state	Gap (eV)	T_C (K)	E_{Form} (eV/atom)	$E_{Form-ML}$ (eV/atom)
Co_2NbAl	FM	0.594	671	−0.424	−0.401
Co_2CrB	FM	0.385	1066	0.134	0.011
Fe_2CrGe	AFM	0.346	393	−0.041	−0.052
Co_2ScSi	FM	0.223	255	−0.589	−0.582
Co_2ZrAl	FM	0.163	649	−0.520	−0.511
Co_2ZrGa	FM	0.113	584	−0.440	−0.450

For Co_2NbAl and Co_2CrB, with the assistance of DFT calculations, they indicate a good half-metallic FM ground states. Their half-metallic gaps are 0.594 and 0.385 eV, respectively, which are comparable to the famous HM, Co_2MnSi [15]. The spin-polarized band structures and partial density of states (PDOS) are shown in figure 6. The PDOS of majority spin channel is metallic, while minority spin channel is semiconductor-like around the Fermi level, showing the half-metallic behavior. As for Co_2NbAl, the valence band maximum (VBM) in the minority-spin band is located at −0.477 eV and the conduction band minimum (CBM)is at 0.117 eV at G point, thereby the gap is 0.594 eV. As we known, GGA often underestimates the width of the band gap [45], therefore the gap of Co_2NbAl should be bigger than the calculated value. We have highlighted the PDOS of Co *d*, Nb *d* and Al *p* electrons for Co_2NbAl. Below the Fermi energy, the total densities of states (TDOS) are predominantly due to Co *d* electrons and Co atoms have the principle contribution to the total DOS. As for Co_2CrB, VBM is located at −0.202 eV and CBM is at 0.183 eV, thereby the gap is 0.385 eV. As shown in table 4, we found that the formation energy of Co_2CrB is 0.134 eV/atom in OQMD , which means it is very likely to be decomposed in nature. This result largely limits the application of Co_2CrB.

Furthermore, the magnetic exchange interactions could be calculated by mapping the total energy of different magnetic states into a Heisenberg model, further used to estimate the critical temperature:

$$H = -\sum_{ij} J_{ij} S_i \cdot S_j, \tag{5}$$

where S_i and S_j are the spin vectors of Co, Cr ions at the sites i and j in the case of Co_2NbAl. J_{ij} is the exchange interaction between the nearest-neighbor spin pair. The J_{ij} was calculated using the energy difference of three different magnetic structures [FM; AFM-1(1 0 0); AFM-2(1 1 0)]:

$$E_{\mathrm{FM}} = E_0 - 32J_{\mathrm{Co-Nb}}S_{\mathrm{Co}}S_{\mathrm{Nb}} - 24J_{\mathrm{Co-Co}}S_{\mathrm{Co}}S_{\mathrm{Co}}; \tag{6}$$

$$E_{\mathrm{AFM\text{-}1}} = E_0 - 8J_{\mathrm{Co-Co}}S_{\mathrm{Co}}S_{\mathrm{Co}}; \tag{7}$$

$$E_{\mathrm{AFM\text{-}2}} = E_0 + 8J_{\mathrm{Co-Co}}S_{\mathrm{Co}}S_{\mathrm{Co}}. \tag{8}$$

Then, T_{C} can be estimated within the mean-field approximation (MFA) by solving the equation [46, 47]:

$$\langle S_i^z \rangle = \frac{S_i(S_i+1)}{3k_{\mathrm{B}}T} \sum_j J_{ij} \langle S_j^z \rangle . \tag{9}$$

The T_{C} is given by the largest eigenvalue of the matrix

$$\Theta_{ij} = \frac{S_i(S_i+1)}{3k_{\mathrm{B}}} \sum J_{ij} \tag{10}$$

here k_{B} is the Boltzmann constant. The estimated T_{C} results are listed in table 4, in where it is found that the T_{C} of Co_2CrB is as high as 1066 K, followed by Co_2NbAl at 671 K. There must be some differences between the T_{C} calculated by the MFA and the experimental measurement, but such high value implies that the actual T_{C} should be much higher than room temperature. Therefore Co_2NbAl would be a promising FM HM for spintronics application. The T_{C} of Co_2ZrAl, Co_2ZrGa, Fe_2CrGe and Co_2ScSi are 649 K, 584 K, 393 K and 255 K, respectively. Although the ground state of Fe_2CrGe is AFM, the magnetic ground state change generated by the strain might be also a little attractive for applications.

Note that we became aware of similar studies in [48] showing Co_2NbAl and Co_2ZrAl are Half-metallic ferromagnet.

4. Conclusions

To summarize, we have carried out an efficient ML workflow based on DNN for searching thermodynamic stable HSP ferromagnet in Heulser alloys. We used DNN models to screen 10 577 candidate materials and then obtained 192 potentially stable and HSP materials. In addition, Co_2NbAl, Fe_2CrGe, Co_2CrB, Co_2ScSi, Co_2ZrAl and Co_2ZrGa were found to have half-metallic property, which are carefully evaluated using systematically DFT calculations. Moreover, some of them might be potential candidates for spintronic application as its T_{C} is estimated to be much higher than room temperature. In conclusion, our approach based on data of material databases and DNN provides an effective way for discovering the superior half-metallic ferromagnet, which could be applied to other structural families, opening up further possibilities for the discovery of innovative functional materials. In future work, we also encourage the exploration of novel materials using more interpretable machine learning methods to compose similar workflow, such as Random Forests, k-Nearest Neighbor and Kernel Ridge Regression.

5. Data availability

The data sets generated during and/or analyzed during the current study are available from the corresponding author on reasonable request.

6. Code availability

The codes used for preprocessing, model training, and invocation are available from the corresponding author on reasonable request.

Acknowledgments

This work was supported by National Natural Science Foundation of China (Grant Nos. 51572086, 51302085, 51402033 and 11874273), the Key Project of Sichuan Science and Technology Program (No. 2019YFSY0044), the Project of Heibei Educational Department, China (No. ZD2018015), and the Natural Science Foundation of Hebei Province (No. A2019203507).

ORCID iDs

Xiao Hu https://orcid.org/0000-0002-6139-2189
Xin Li https://orcid.org/0000-0002-4903-2789
Zhenjie Zhao https://orcid.org/0000-0001-5366-4896

References

[1] Wolf S A *et al* 2001 Spintronics: a spin-based electronics vision for the future *Science* **294** 1488–95
[2] Pickett W E and Moodera J S 2001 Half metallic magnets *Phys. Today* **54** 39–44
[3] Irkhin V Yu *et al* 2008 Half-metallic ferromagnets: from band structure to many-body effects *Rev. Mod. Phys.* **80** 315–78
[4] Jianhua Ma *et al* 2018 Computational investigation of inverse heusler compounds for spintronics applications *Phys. Rev.* B **98** 094410
[5] Chioncel L, Arrigoni E, Katsnelson M I and Lichtenstein A I 2006 Electron correlations and the minority-spin band gap in half-metallic heusler alloys *Phys. Rev. Lett.* **96** 137203
[6] Gao G Y *et al* 2007 Half-metallic ferromagnetism in zinc-blende CaC, SrC, and BaC from first principles *Phys. Rev.* B **75** 174442
[7] Coey J M D and Venkatesan M 2002 Half-metallic ferromagnetism: example of Cro_2 (invited) *J. Appl. Phys.* **91** 8345–50
[8] Tobin J G *et al* 2007 Spin resolved photoelectron spectroscopy of Fe_3O_4: the case against half-metallicity *J. Phys.: Condens. Matter* **19** 315218
[9] Jedema F J, Filip A T and van Wees B J 2001 Electrical spin injection and accumulation at room temperature in an all-metal mesoscopic spin valve *Nature* **410** 345–8
[10] Graf T, Felser C and Parkin S S P 2011 Simple rules for the understanding of heusler compounds *Prog. Solid State Chem.* **39** 1–50
[11] de Groot R A *et al* 1983 New class of materials: half-metallic ferromagnets *Phys. Rev. Lett.* **50** 2024–7
[12] Graf T *et al* 2013 *Chapter One—Magnetic Heusler Compounds* vol 21 (Amsterdam: Elsevier)
[13] Chadov S *et al* 2010 Tunable multifunctional topological insulators in ternary heusler compounds *Nat. Mater.* **9** 541
[14] Ishida S *et al* 1995 Search for half-metallic compounds in Co_2MnZ (Z = IIIb, IVb, Vb element) *J. Phys. Soc. Japan* **64** 2152–7
[15] Picozzi S, Continenza A and Freeman A J 2002 Co_2MnX (X = Si, ge, sn) heusler compounds: an *ab initio* study of their structural, electronic, and magnetic properties at zero and elevated pressure *Phys. Rev.* B **66** 094421
[16] Sanvito S *et al* 2017 Accelerated discovery of new magnets in the heusler alloy family *Sci. Adv.* **3** 1602241
[17] Jain A *et al* 2013 Commentary: The materials project: A materials genome approach to accelerating materials innovation *APL Mater.* **1** 011002
[18] Curtarolo S *et al* 2012 Aflowlib.org: a distributed materials properties repository from high-throughput *ab initio* calculations *Comput. Mater. Sci.* **58** 227–35
[19] Kirklin S *et al* 2015 The open quantum materials database (oqmd): assessing the accuracy of dft formation energies *NPJ Comput. Mater.* **1** 15010
[20] Zheng X, Zheng P and Zhang R-Z 2018 Machine learning material properties from the periodic table using convolutional neural networks *Chem. Sci.* **9** 8426–32
[21] Gao Q, Opahle I and Zhang H 2019 High-throughput screening for spin-gapless semiconductors in quaternary heusler compounds *Phys. Rev. Mater.* **3** 024410
[22] Kim K *et al* 2018 Machine-learning-accelerated high-throughput materials screening: discovery of novel quaternary heusler compounds *Phys. Rev. Mater.* **2** 123801
[23] Lindmaa A *et al* 2016 Machine learning energies of 2 million elpasolite (ABC_2D_6) crystals *Phys. Rev. Lett.* **117** 135502
[24] Snyder J C, Rupp M, Hansen K, Müller K-R and Burke K 2012 Finding density functionals with machine learning *Phys. Rev. Lett.* **108** 253002
[25] Legrain F *et al* 2018 Materials screening for the discovery of new half-heuslers: machine learning versus *ab initio* methods *J. Phys. Chem.* B **122** 625–32
[26] Oliynyk A O *et al* 2016 High-throughput machine-learning-driven synthesis of full-heusler compounds *Chem. Mater.* **28** 7324–31
[27] Takahashi K and Tanaka Y 2017 Unveiling descriptors for predicting the bulk modulus of amorphous carbon *Phys. Rev.* B **95** 054110
[28] Grossman J C and Xie T 2018 Crystal graph convolutional neural networks for an accurate and interpretable prediction of material properties *Phys. Rev. Lett.* **120** 145301
[29] Segler M H S, Preuss M and Waller M P 2018 Planning chemical syntheses with deep neural networks and symbolic ai *Nature* **555** 604
[30] Ye W *et al* 2018 Deep neural networks for accurate predictions of crystal stability *Nat. Commun.* **9** 3800
[31] Balachandran P V *et al* 2018 Predictions of new ABO_3 perovskite compounds by combining machine learning and density functional theory *Phys. Rev. Mater.* **2** 043802
[32] Hill J *et al* 2016 Materials science with large-scale data and informatics: unlocking new opportunities *MRS Bull.* **41** 399C409
[33] Ueno T *et al* 2016 Combo: an efficient bayesian optimization library for materials science *Mater. Discovery* **4** 18–21
[34] Bartel C J *et al* 2018 Physical descriptor for the gibbs energy of inorganic crystalline solids and temperature-dependent materials chemistry *Nat. Commun.* **9** 4168
[35] Kingma D P and Ba J 2014 Adam: a method for stochastic optimization *3rd International Conference for Learning Representations* (arXiv:1412.6980)
[36] Blöchl P E 1994 Projector augmented-wave method *Phys. Rev.* B **50** 17953–79
[37] Kresse G and Furthmller J 1996 Efficiency of *ab initio* total energy calculations for metals and semiconductors using a plane-wave basis set *Comput. Mater. Sci.* **6** 15–50
[38] Perdew J P, Burke K and Ernzerhof M 1996 Generalized gradient approximation made simple *Phys. Rev. Lett.* **77** 3865–8
[39] Curtarolo S *et al* 2013 The high-throughput highway to computational materials design *Nat. Mater.* **12** 191
[40] Hart G L W, Curtarolo S, Massalski T B and Levy O 2013 Comprehensive search for new phases and compounds in binary alloy systems based on platinum-group metals, using a computational first-principles approach *Phys. Rev.* X **3** 041035
[41] Coey J M D and Sanvito S 2004 Magnetic semiconductors and half-metals *J. Phys. D: Appl. Phys.* **37** 988–93
[42] Djeghloul F *et al* 2013 Direct observation of a highly spin-polarized organic spinterface at room temperature *Sci. Rep.* **3** 1272
[43] Mazin I I 1999 How to define and calculate the degree of spin polarization in ferromagnets *Phys. Rev. Lett.* **83** 1427–30

[44] Balluff J *et al* 2017 High-throughput screening for antiferromagnetic heusler compounds using density functional theory *Phys. Rev. Mater.* **1** 034404
[45] Perdew J P *et al* 1999 Accurate density functional with correct formal properties: a step beyond the generalized gradient approximation *Phys. Rev. Lett.* **82** 2544–7
[46] Anderson P W 1963 *Theory of Magnetic Exchange Interactions: Exchange in Insulators and Semiconductors* vol 14 (New York: Academic)
[47] Şaşıoğlu E, Sandratskii L M and Bruno P 2004 First-principles calculation of the intersublattice exchange interactions and curie temperatures of the full heusler alloys Ni_2MnX ($X = Ga, In, Sn, Sb$) *Phys. Rev.* B **70** 024427
[48] Ghosh S and Ghosh S 2019 Systematic understanding of half-metallicity of ternary compounds in heusler and inverse heusler structures with 3d and 4d elements *Physica Scripta* **94** 125001